

# A New Motion Management Method for Lung Tumor Tracking Radiation Therapy

NORIYASU HOMMA  
Tohoku University  
Cyberscience Center  
6-6-05 Aoba, Aoba-ku  
Sendai 980-8579  
JAPAN  
homma@ieee.org

MASAO SAKAI  
Tohoku University  
Center Inform. Tech. Edu.  
41 Kawauchi, Aoba-ku  
Sendai 980-8576  
JAPAN  
sakai@he.tohoku.ac.jp

HARUNA ENDO  
Tohoku University  
Graduate School of Medicine  
2-1 Seiryomachi, Aoba-ku  
Sendai 980-8575  
JAPAN  
endo@yoshizawa.ecei.tohoku.ac.jp

MASATOSHI MITSUYA  
Tohoku University  
Graduate School of Medicine  
2-1 Seiryomachi, Aoba-ku  
Sendai 980-8575  
JAPAN  
m-mitsuya@mwc.biglobe.ne.jp

YOSHIHIRO TAKAI  
Tohoku University  
Graduate School of Medicine  
2-1 Seiryomachi, Aoba-ku  
Sendai 980-8575  
JAPAN  
y-takai@mail.tains.tohoku.ac.jp

MAKOTO YOSHIZAWA  
Tohoku University  
Cyberscience Center  
6-6-05 Aoba, Aoba-ku  
Sendai 980-8579  
JAPAN  
yoshizawa@ieee.org

*Abstract:* We propose a new motion management method for lung tumor tracking radiotherapy by using a novel time series prediction technique. In radiotherapy, the target motion often affects the conformability of the therapeutic dose distribution delivered to thoracic and abdominal tumors, and thus tumor motion monitoring systems have been developed. Even we can observe tumor motion accurately, however, radiotherapy systems may inherently have mechanical and computational delays to be compensated for synchronizing dose delivery with the motion. For solving the delay problem, we develop a novel system to predict complex time series of the lung tumor motion. An essential core of the system is an adaptive prediction modeling with a phase locking technique by which time-varying cyclic dynamics is transferred into a time invariant one. Simulation studies demonstrate that the proposed system can achieve a clinically useful high accuracy and long-term prediction of the average error  $1.05 \pm 0.99$  [mm] at 1 [sec] ahead prediction.

*Key-Words:* Time series prediction, adaptive modeling, radiation therapy, lung tumor, and motion management.

## 1 Introduction

It is important for radiation therapy to give sufficient dose to tumor and to reduce normal tissue toxicity. By using image-guided techniques, extracranial stereotactic radiotherapy (ESRT) can achieve a precise dose delivery in a short time [1] and thus have a good outcome that is comparable to the performance of surgery [2]. In addition to this, delivering a highly conformal dose distribution to a “static” tumor target in three-dimensional space is largely solved by techniques such as intensity modulated radiation therapy (IMRT) [3, 4].

In radiation therapy, it is known that the target motion often affects the conformability of the therapeutic dose distribution delivered to thoracic and abdominal tumors. Tumor motions can not only be associated with patient’s stochastic movements and systematic drifts, but also involve internal movements caused by such as respiration and cardiac cycles [5].

To take into account such “dynamic” nature of the internal organ motion during the course of radia-

tion therapy, several techniques have been proposed and evaluated in clinical use. A simple method is to increase the planning target volume (PTV) to cover the possible range of motion of the target [6], but undesirably it results in an increased dose to the normal tissues surrounding the tumor. One of the other methods to treat the respiratory motion of the lung tumor is a breath-hold technique [7]. Since the respiration may be dominant over the lung tumor motion, the tumor can be regarded as a static target by using such technique to stop the respiration. Geometric gating method is also this kind of techniques to limit the motion effect [8, 9, 10, 11]. They are, however, not desirable techniques because of patient intervention by the breath-hold or beam interruption by the gating. In this sense, tumor tracking by moving the radiation source [12, 13, 14] or the beam defined by multileaf collimator [15, 16, 17] can be in an ideal direction.

To achieve such tumor tracking, several methods have been proposed. Among these, direct measurements of a fiducial gold marker of the tumor position by fluoroscopy imaging techniques [18, 19, 20,

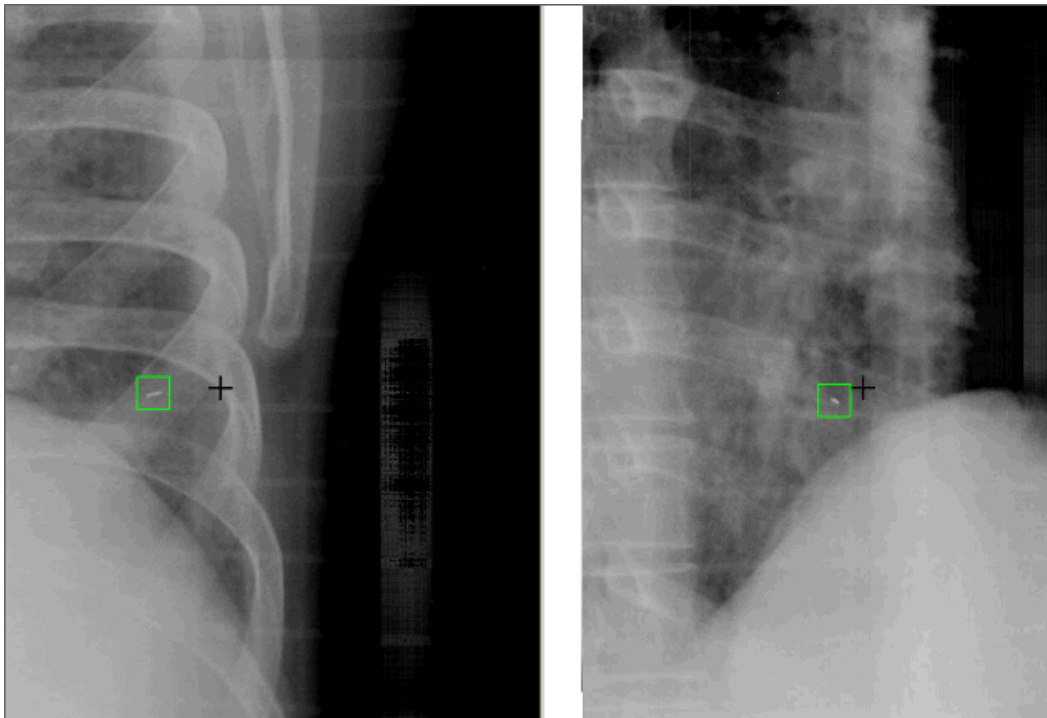


Figure 1: An example of X-ray images of the fiducial gold marker implanted into a lung tumor. Three-dimensional coordinates of the tumor motion can be measured by using the marker's position.

21, 22], as shown in Fig. 1 for example, are more promising than indirect ones such as external skin marker tracking [11, 23, 24] and breath monitoring techniques [25]. Such tracking systems may involve mechanical and computational delays to control the multileaf collimator and for image and time series processings of the tumor motion. Thus, the time delay must be compensated by predicting the tumor motion to accomplish a real-time tracking [5]. The desired accuracy of the tumor location can be within about 1 [mm] at up to 1 [sec] ahead prediction. This is a highly accurate condition for the complex dynamics of the tumor motion.

In this paper, we propose a new system realizing such highly accurate prediction of lung tumor motion for tracking radiation therapy. The proposed system takes into account the complex dynamics by using an adaptive modeling for the prediction.

The rest of this paper consists of as follows. We will investigate nature of the motion first, by using time series analysis techniques in section 2. Then prediction method will be developed in section 3 by using results of the analysis. In section 4, prediction accuracy of the proposed system will be evaluated by using real data of tumor motions in which the performances of the prediction systems consisting of a smoothing prediction model designed by Holt-Winters seasonal (HWS) method [26] and more general seasonal ARIMA (SARIMA) model [27] are compared to a conventional prediction method. Con-

cluding remarks will be given in section 5.

## 2 Motion of Lung Tumor

Three-dimensional time series of human lung tumor motion was observed at Hokkaido University Hospital [28]. An example of the tumor location at superior segment of right lung, S6, is shown in Fig. 2. A dominant source of the tumor motion is respiration, but the others such as caused by cardiac motion may also be included in the time series.

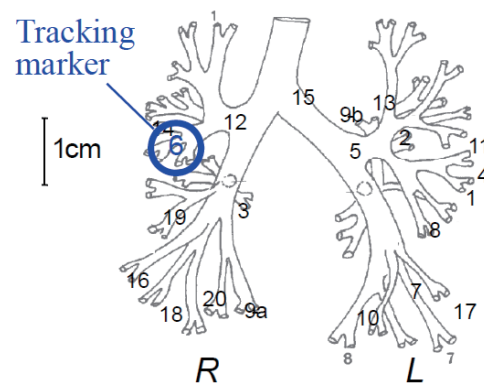


Figure 2: Structure of a human lung.

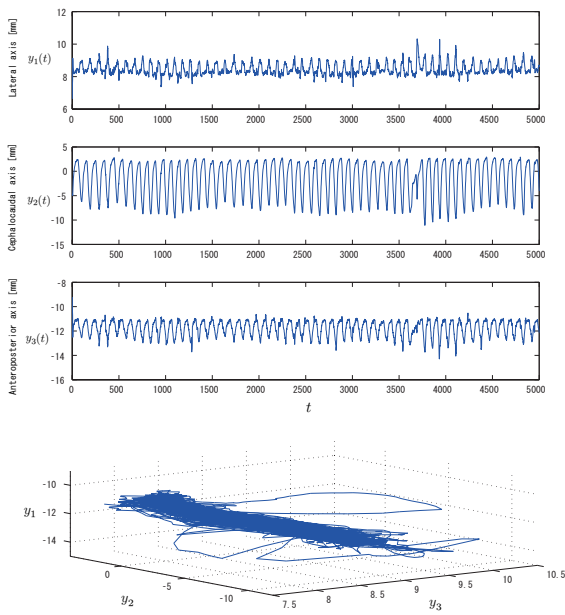


Figure 3: Preprocessed time series  $\mathbf{y}(t)$  of the observed tumor marker motion at S6 of the lung.

### 2.1 Preprocessing (noise reduction) of the time series

A fiducial gold marker implanted into the lung tumor was used to measure the three-dimensional coordinates of the tumor motion. The spatial resolution and sampling period were 0.01[mm] and 0.033[sec] (30[Hz]), respectively. To reduce observational noise and avoid abnormal data involved in raw data of the time series, we preprocessed the time series by using several filters such as the Kalman filter [29] and statistical filters. An example of the preprocessed time series

$$\mathbf{y}(t) = [y_1(t) \ y_2(t) \ y_3(t)] \quad (1)$$

$t = 1, 2, \dots, 5000$ , are shown in Fig. 3. Here elements of vector  $\mathbf{y}(t)$  at time  $t$  [step],  $y_1(t)$ ,  $y_2(t)$ , and  $y_3(t)$  [mm], are the marker's position of the lateral, cephalocaudal, and anteroposterior directions, respectively. Note that the time series of the vector  $\mathbf{y}(t)$ ,  $t = 1, 2, \dots$ , can be obtained in real-time.

For the teaching data of time series prediction, we further reduced the observational impulse noise involved in the time series  $\mathbf{y}(t)$ ,  $t = 1, 2, \dots$ , in Eq. (1) by using statistical filters, and then reduced high frequency noise by using a low pass filter that deletes unnecessary high frequency components that are higher than  $0.1 \times f_{\max}$  [Hz]. Here  $f_{\max}$  is the maximum frequency of the digital Fourier transform spectrum under the sampling period. The statistics can be computed by using all data of the time series for  $t = 1, 2, \dots, 5000$  in Fig. 3. The noise reduced time series  $\mathbf{y}^*(t) = [y_1^*(t) \ y_2^*(t) \ y_3^*(t)]$  are shown in Fig. 4 and assumed as the real motion of the fiducial

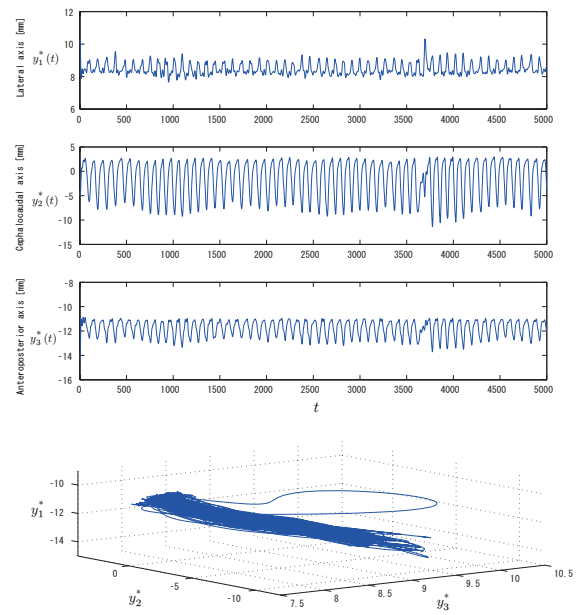


Figure 4: The noise reduced time series  $\mathbf{y}^*(t)$  of the marker motion.

marker of the tumor.

### 2.2 Cyclic dynamics

There can be cyclic dynamics with approximately 90 [steps] periods of respiratory motion involved in the fiducial marker motion of the lung tumor as seen in Figs. 3 and 4. Note that the periods of the cyclic components and rhythmic dynamics can be fluctuated when the respiratory dynamics are changed. If patients are in rest, however, respiratory dynamics is almost cyclic and thus the dominant dynamics of time series is also cyclic as seen in Fig. 3.

We calculate the autocorrelation function (ACF),  $\gamma$ , of the time series for further analysis of the cyclic dynamics involved in the tumor motion. Fig. 5 shows  $\gamma(t, k)$  of a sample time series in the cephalocaudal direction,  $[y_2^*(t - 150) \ y_2^*(t - 149) \ \dots \ y_2^*(t + 149) \ y_2^*(t + 150)]$ , within a time window (301 steps) as

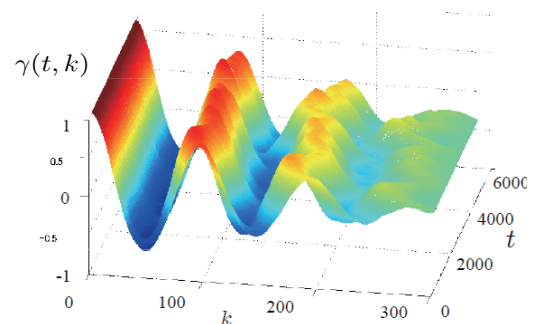


Figure 5: Autocorrelation function,  $\gamma(t, k)$ , of  $y_2^*$ .

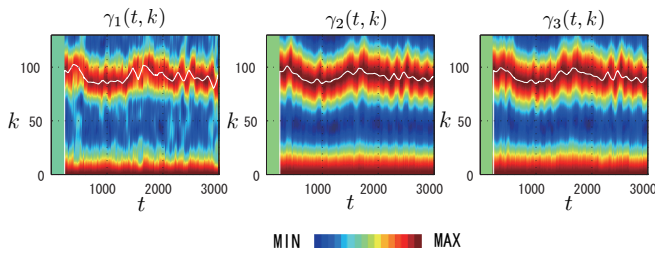


Figure 6: Autocorrelation functions of  $Y(t)$ .

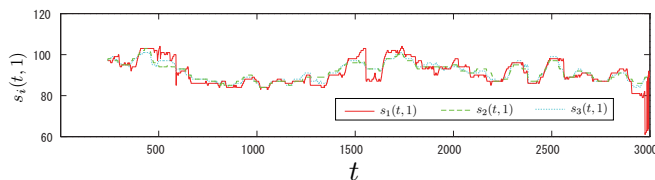


Figure 7: Periods  $s_i$ ,  $i = 1, 2, 3$ , of  $Y(t)$  as functions of time  $t$ . It can be seen that periods are slightly fluctuated around  $s_i = 90$ .

a function of time  $t$  [step] and the shift  $k$  [step]. Note that the first peak of the ACF at a shift  $k(\geq 1)$  corresponds to the dominant period of the cyclic dynamics. Then from the autocorrelation function analysis, it is revealed that the dominant periods are approximately 90 [steps] as expected above. Furthermore, the periods are slightly and smoothly fluctuated and thus they can be time variant. As shown in Figs. 6 and 7, ACFs for time series of the other two directions,  $y_1^*$  and  $y_3^*$ , are almost similar to that of  $y_2^*$ .

In the following section, we will build a model with time variant periods for predicting such fluctuated motion of the lung tumor.

### 3 Prediction Method

#### 3.1 Concept of prediction algorithm

Fig. 8 shows a tumor motion prediction system proposed in this paper. Let us predict the  $h$ -step ( $h \geq 1$ ) ahead fiducial marker's position of the lung tumor.

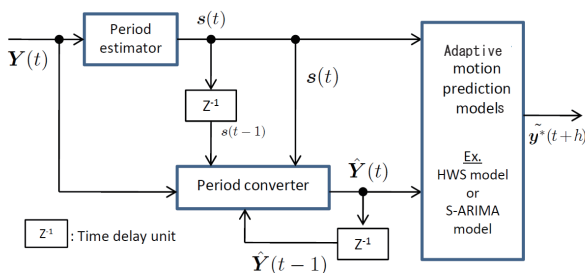


Figure 8: The proposed prediction system.

The predicted position  $\hat{y}^*(t+h)$  of the actual (noise reduced) tumor position  $y^*(t+h)$  is calculated by using the real-time preprocessed time series available at time  $t$

$$Y(t) = [y(1) \ y(2) \ \dots \ y(t-1) \ y(t)]^T \quad (2)$$

Basic ideas of the prediction algorithm are as follows. As analyzed in section 2.2, the target time series  $y^*(t)$  may include a complex dynamics with time variant periods. Thus, far past information involved in the whole time series  $Y(t)$  is less important or even can have a bad effect on the prediction accuracy. Then, the prediction model can be built based on the not far past information of the time series. Note that the current period is one of the most important piece of information for the prediction because the cyclic dynamics makes the prediction be precise. In this sense, the proposed algorithm tries to estimate the current dominant period as precise as possible by using a fresh piece of information involved in the current time series available.

Let us consider the current period vector  $s^*(t) = [s_1^*(t) \ s_2^*(t) \ s_3^*(t)]$  of the time series  $y^*(t) = [y_1^*(t) \ y_2^*(t) \ y_3^*(t)]$  at time  $t$ , and denote its estimation as  $s(t) = [s_1(t) \ s_2(t) \ s_3(t)]$ . The estimation of the  $s^*$  can be calculated by using the autocorrelation function analysis of a fresh sample time series with a time length  $L$  given as  $y_i(\tau), \tau = t-L, t-L+1, \dots, t$ , available at time  $t$ . To use the important piece of information included in the fresh sample of the time series,  $L$  can cover time series for more than the current period in time length,  $s_i(t-1) < L$ , but should not be too large as mentioned above. Here if the estimated period is changed,  $s_i(t-1) \neq s_i(t)$ , then the model of cyclic dynamics is adapted to the new current period  $s_i(t)$ . The final  $h$ -step ahead prediction  $\hat{y}^*(t+h)$  can be calculated based on the adapted model of the new cyclic dynamics  $\hat{Y}(t)$  as shown in Fig. 8.

#### 3.2 Prediction model

As prediction models of the lung tumor motion that is mainly caused by the respiration with time variant cyclic periods, we adopt two models of the time series here. One is Holt-Winters exponential smoothing, a smoothing model designed by the HWS method, and the other is a seasonal ARIMA (SARIMA) model. Note that, however, any other linear or nonlinear models including neural networks can be incorporated into the proposed adaptive prediction method.

##### 3.2.1 Holt-Winters exponential smoothing

The HWS method can provide an easy design of the seasonal model to predict 1-step ahead of the time

series if the period of cyclic dynamics is known and time invariant. The general formulations of the HWS is given as follows.

$$\tilde{y}_i^*(t+h) = a_i(t) + b_i(t)h + c_i(t-h + \text{mod}(h, s_i(t))) \quad (3)$$

$$a_i(t) = \alpha(y_i(t) - c_i(t)) + (1-\alpha)(a_i(t-1) + b_i(t)) \quad (4)$$

$$b_i(t) = \beta(a_i(t) - a_i(t-1)) + (1-\beta)(b_i(t-1)) \quad (5)$$

$$c_i(t) = \gamma(y_i(t) - a_i(t)) + (1-\gamma)(c_i(t-s_i(t))) \quad (6)$$

where the initial values at time  $t_0 (> s_i(t_0))$  can be initialized by

$$a_i(t_0) = y_i(t_0) \quad (7)$$

$$b_i(t_0) = \frac{y_i(t_0) - y_i(t_0 - s_i(t_0) + 1)}{s_i(t_0)} \quad (8)$$

$$c_i(t_0 - k) = y_i(t_0 - k) - (y_i(t_0 - s_i(t_0) + 1) + (s_i(t_0) - k) \cdot b_i(t_0)) \dots k = 0, 1, 2, \dots, s_i(t_0) \quad (9)$$

In such case, only three smoothing parameters, implying the ratio of use the predicted data to the previous actual data for smoothing, may be designed as values between 0 and 1; 0 implies smoothing by only the actual data, while 1 implies smoothing by only the predicted data. The three parameters,  $0 \leq \alpha, \beta, \gamma \leq 1$ , are ratios for smooth calculation of the trend level, the gradient of trend, and cyclic component, respectively.

On the other hand, the easy design restricts freedom of the model and thus the prediction accuracy is limited in the case of complicated time series. Also, modeling errors may be accumulated for a mid- or long-term prediction ( $h \gg 1$ ) and the prediction will result in failure with a large error beyond the tolerance.

### 3.2.2 Seasonal ARIMA model

The other model, the general SARIMA model of the time series,  $[x(0) x(1) \dots x(t)]$ , with period  $s$  [steps] of cyclic dynamics can be given as follows.

$$\phi(B)\Phi(B^s)(1-B)^d(1-B^s)^D x(t) = \theta(B)\Theta(B^s)e(t) \quad (10)$$

$$\phi(z) = 1 - \phi_1 z - \phi_2 z^2 - \dots - \phi_p z^p \quad (11)$$

$$\Phi(z) = 1 - \Phi_1 z - \Phi_2 z^2 - \dots - \Phi_P z^P \quad (12)$$

$$\theta(z) = 1 + \theta_1 z + \theta_2 z^2 + \dots + \theta_q z^q \quad (13)$$

$$\Theta(z) = 1 + \Theta_1 z + \Theta_2 z^2 + \dots + \Theta_Q z^Q \quad (14)$$

where  $e(t)$  is the Gaussian noise of which average and variance are 0 and  $\sigma^2$ , respectively.  $B$  is a time delay operator defined as

$$B^k x(t) = x(t-k)$$

The parameters  $d, D, p, P, q,$  and  $Q$  represent dimensions of corresponding terms, respectively. Because of high degree of design parameter freedom of the SARIMA model, the model can predict complicated dynamics with a high precision. It is often, however, hard to design such appropriate parameters of the model for the precise prediction.

To design the SARIMA model, we first make a compensated time series  $x(t)$  from the adapted pre-processed time series  $\hat{y}(t)$  as

$$x(t) = \hat{y}(t) - z(t) \quad (15)$$

where  $z(t) = [z_1(t) z_2(t) z_3(t)]$  is a trend level vector at time  $t$  of the time series  $\hat{y}(t)$  defined by

$$z_i(t) = \frac{1}{s_i(t)} \sum_{\tau=t-s_i(t)+1}^t \hat{y}_i(\tau) \quad (16)$$

$i = 1, 2, 3$ . Then, the SARIMA model can be build by using the compensated time series with a time length of  $L$  given as

$$X(t) = [x(t-L) x(t-L+1) \dots x(t)]^T \quad (17)$$

For avoiding the accumulation of the modeling error at each step, we directly design an  $h$ -step ahead prediction model instead of repeatedly use of the 1-step ahead prediction one. To this end, the following constraint can be introduced.

$$\phi_i = 0 \dots \text{if } \text{mod}(i, [h/2]) \neq 0 \quad (18)$$

where  $[x]$  denotes an operator that gives maximum integer not greater than  $x$  and  $\text{mod}(i, k)$  gives the remainder on division of  $i$  by  $k$ .

## 4 Results and Discussions

### 4.1 Adaptive compensation

The estimation of the current dominant periods of cyclic dynamics was conducted during prediction for the model adaptation. The estimation results are shown in Figs. 9 and 10. As seen in these figure, estimated periods as functions of time converge in around 90 after 600 steps. A reason why such long (600) steps were needed for convergence of the estimated periods may be due to the limitation of the changes of the estimated periods given as  $|s_i(t) - s_i(t-1)| \leq 1, i = 1, 2, 3$ , with the initial values  $s_i(0) = 1$  to

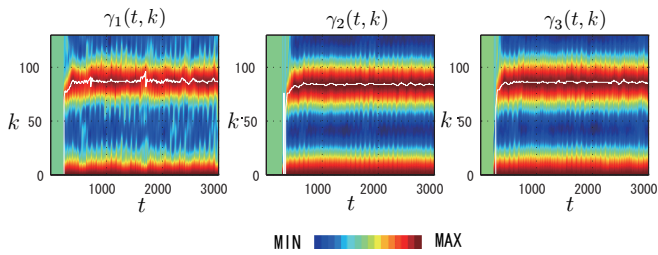


Figure 9: Autocorrelation functions of the compensated time series  $\hat{Y}(t)$ .

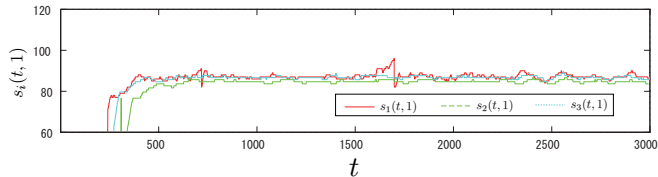


Figure 10: Periods  $s_i$ ,  $i = 1, 2, 3$ , of the compensated time series  $\hat{Y}(t)$  as functions of time  $t$ . Compared to Figs. 6 and 7, the compensated periods are almost constant after the convergence ( $t > 600$ ).

avoid undesirable oscillation of the estimation by radical changes of the estimation. This may, however, require only additional 20 [sec] observations before the actual therapeutic irradiation in clinical use.

On the other hand, compared to Figs. 6 and 7, the periods of the compensated time series are almost constant after the convergence. Fig. 11 shows superimposition of the time series for each compensated period on the phase axis by using the period estimated. Compared to the original time series, the phases (wave shapes) of the compensated time series for different periods are synchronized with each other. As is clear from these figures, the proposed compensation is effective for the phase synchronization of the fluctuated time series.

## 4.2 Prediction results

We have tested the proposed system using a prediction task in which the preprocessed time series  $Y(t)$  of fiducial marker's motions of several lung tumors are used. To evaluate the performance under the worst (longest-term) condition required in clinical use, the maximum length of  $h = 30$ -step (1 [sec]) ahead prediction was conducted first.

An example of the resulting time series for  $t = 3000$  to  $5000$  predicted by the smoothing model designed by the HWS method is shown in Fig. 12. In this result, the smoothing parameters were experimentally designed as  $\alpha = 0.01$ ,  $\beta = 0.05$ , and  $\gamma = 0.7$ , respectively.

On the other hand, for the same target time series,

the prediction result by the adaptive SARIMA model is shown in Fig. 13. Here, the objective prediction steps  $h = 30$  is a mid- or long- term. In this case, to avoid the overfitting problem for the model design, we simplified the model as  $d = D = q = Q = 0$ , and experimentally designed as the rest of the dimensional parameters  $p = 5h$  and  $P = 6s_i(t)$ , respectively. Referential time series predicted by the zero-order hold model given as  $\tilde{y}^*(t + h) = y(t)$  are also shown in Figs. 12 and 13. Note that the parameters of both models can be optimized by using some criteria such as Akaike's Information Criterion (AIC) [30].

As is clear from these figures, it can be concluded that prediction accuracy of both smoothing and adaptive SARIMA models is superior to that of the zero-order hold model, and the SARIMA model is slightly further superior to the smoothing model.

To further clarify the effect of the adaptation to the fluctuated periods, we have compared the normal SARIMA and the adaptive SARIMA models. For simplicity, we changed only one parameter  $P$  and the rest of the parameters were  $d = D = p = q = Q = 0$ . Then,  $\Phi_k = 1/P$ ,  $k = 1, 2, \dots, P$ .

Table 1 summarizes prediction errors at 1 [sec] ahead by both SARIMA models with the parameter  $P = 1, 2, \dots, 5$ . First, the results show that the errors by the adaptive SARIMA model is less than the normal SARIMA model for all cases of  $P = 2, 3, 4, 5$ . In other words, the adaptive SARIMA is superior than the normal one. For  $P = 1$ , there is no difference between the normal and adaptive SARIMA models since no compensation is conducted for the time series for the current period.

Second,  $P = 2$  is the optimal condition for  $1 \leq P \leq 5$ . This suggests that there is the optimal length of the time series including a useful piece of information for the prediction. Less or more length of the time series can affect badly on the prediction error as discussed in section 3.1. The condition  $P = 2$  is generally a reasonable for SARIMA model [31]. Thus, the comparison demonstrates the effect of real-

Table 1: The prediction errors (mean  $\pm$  SD) at 1 [sec] (=30 steps) ahead by the normal SARIMA and adaptive SARIMA with  $P = 1, 2, \dots, 5$ .

| $P$ | Normal SARIMA                         | Adaptive SARIMA                       |
|-----|---------------------------------------|---------------------------------------|
| 1   | 1.0954 $\pm$ 0.9984                   |                                       |
| 2   | <b>1.0690 <math>\pm</math> 0.9766</b> | <b>1.0497 <math>\pm</math> 0.9947</b> |
| 3   | 1.2225 $\pm$ 1.1656                   | 1.1175 $\pm$ 1.0242                   |
| 4   | 1.4166 $\pm$ 1.3576                   | 1.2201 $\pm$ 1.1166                   |
| 5   | 1.6112 $\pm$ 1.4736                   | 1.2884 $\pm$ 1.1954                   |

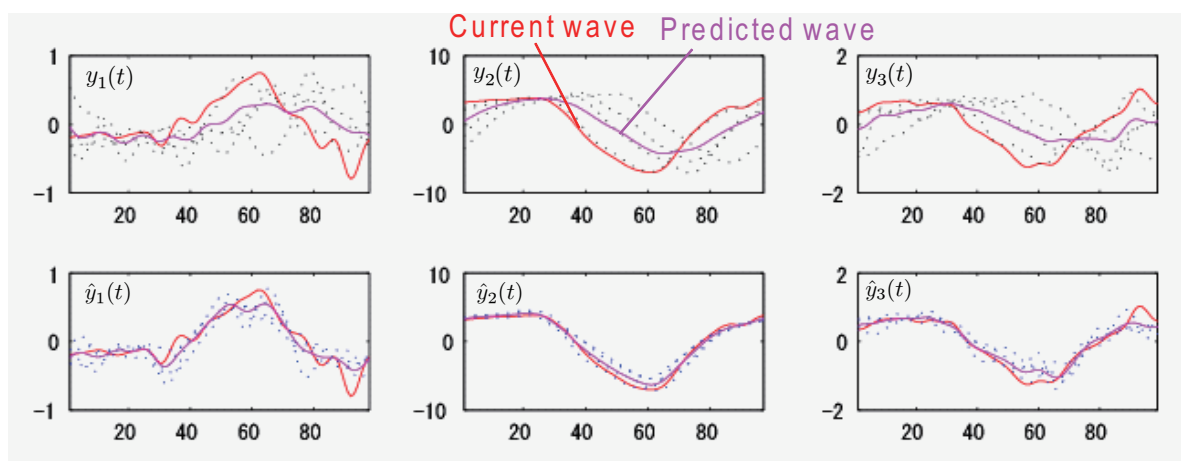


Figure 11: Superimposition of wave shapes of time series for each period. Upper and lower columns show wave shapes of the original time series  $Y(t)$  and the compensated time series  $\hat{Y}(t)$ , respectively. All the periods for  $\hat{Y}(t)$  were compensated to  $s_i = 90$  in this case. Red and purple lines indicate the wave shapes of the current and predicted periods, respectively.

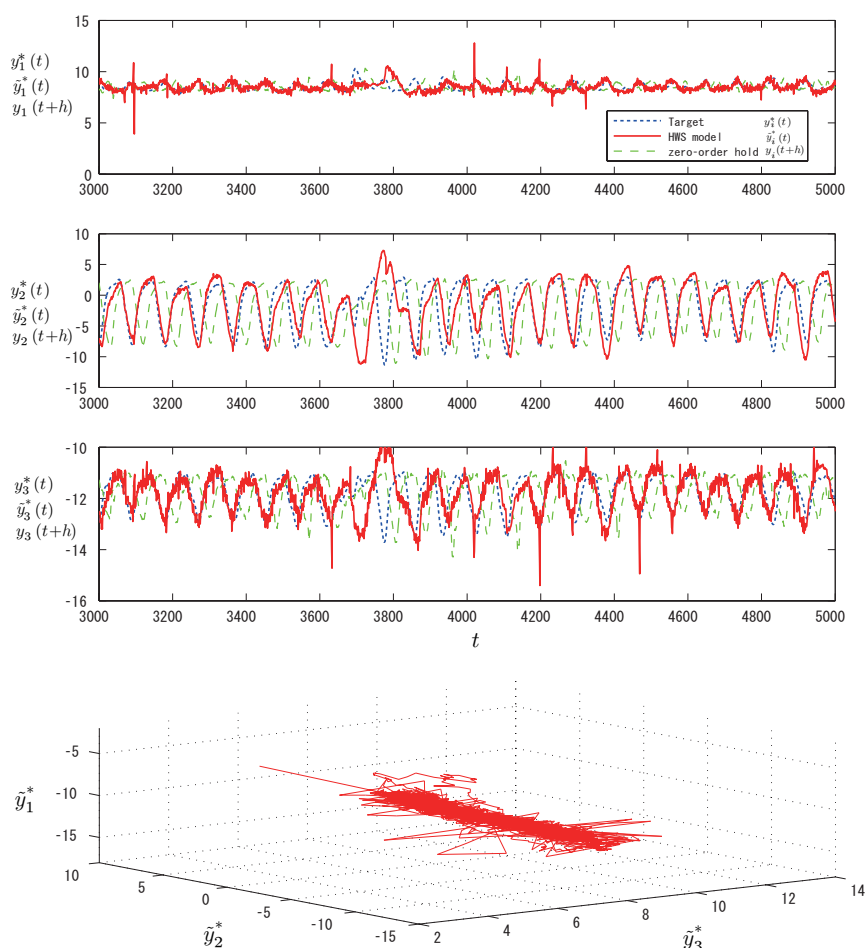


Figure 12: Comparison of time series between the target (blue dotted lines) and the predictions (red lines) at 1 [sec] (30 steps) ahead by the HWS model.

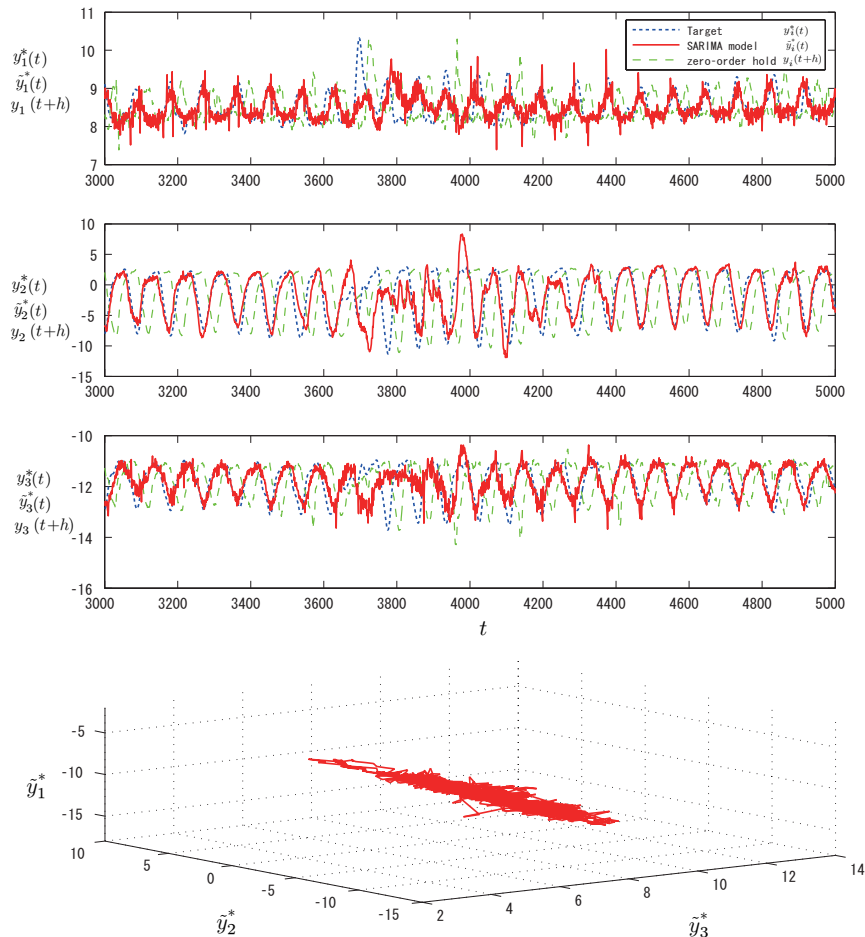


Figure 13: Comparison of time series between the target (blue dotted lines) and the predictions (red lines) at 1 [sec] (30 steps) ahead by the proposed system with SARIMA model.

time adaptation of the model according to the estimated time variant period. The best average error and its standard deviation of the 30-step ahead prediction were  $1.05 \pm 0.99$  [mm], and achieved by the adaptive SARIMA model. What should be stressed here is that this accuracy can be sufficient for clinical use in which the margin of the dose distribution is about 1 millimeter.

In addition, due to nonlinear nature of the respiratory motion, better performance for *short-term predictions* by neural network models compared to linear filters has been reported [32, 33]. Consequently, much better performance for *long-term predictions* can be expected by using any nonlinear models including neural networks [34, 35] and other models such as presented in [36] with the proposed adaptation algorithm for time variant nature.

To further verify this effect of adaptation for shorter- and longer-term predictions, we have evaluated average prediction errors for various  $h$ -step ( $1 \leq h \leq 120$ ) ahead prediction tasks. Fig. 14 shows the average prediction errors as functions of the prediction interval  $h$ , ( $1 \leq h \leq 120$ ). For a wide range of  $h$ ,

(almost all, except for small  $h$ ), prediction accuracy of both the smoothing and SARIMA models was superior to that of the zero-order hold model as expected. The prediction error become larger as the prediction

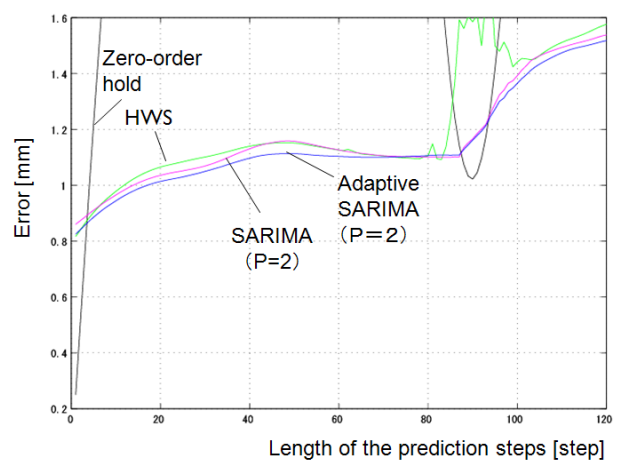


Figure 14: Average errors as functions of the prediction interval  $1 \leq h \leq 120$  [steps].

intervals increase, but the best accuracy was again achieved by the adaptive SARIMA model. It can be concluded that prediction accuracy within 1 [mm] by the adaptive SARIMA model for shorter than 1 [sec] ahead prediction is a promising result for clinical use.

## 5 Conclusions

In this paper, we have developed time series prediction system for lung tumor motion tracking radiation therapy. The precise prediction was achieved by the proposed technique based on the real-time adaptation to the time variant period involved in the cyclic dynamics of respiration that may be a dominant source of the tumor motion. It is expected that such precise prediction will reduce the adverse dosimetric effect of the tumor motion.

Simulation studies revealed the superior prediction performance of the proposed adaptation models compared to the conventional zero-order hold model and that the prediction accuracy may be sufficient for the clinical use. In addition to this, the fact that the performance of the proposed adaptive SARIMA model was further superior to that of the conventional SARIMA suggests the effectiveness of the proposed adaptation technique based on the prediction with high accuracy.

**Acknowledgements:** This work was partially supported by The Ministry of Education, Culture, Sports, Science and Technology under Grant-in-Aid for Scientific Research #19500413. Also, authors would like to thank Dr. Shirato and his colleague at Hokkaido University Hospital for sharing the clinical time series data of human lung motion with us.

### References:

- [1] Wambersie A, Torsten Landberg, T, ICRU Report 62, Prescribing, Recording and Reporting Photon Beam Therapy (Supplement to ICRU Report 50), ICRU News 1999.
- [2] Onishi H, Araki T, Shirato H, et al., Stereotactic hypofractionated high-dose irradiation for stage I nonsmall cell lung carcinoma, *Cancer*, vol. 101, no. 7, pp. 1623-1631, 2004.
- [3] G. A. Ezzell *et al.*, "Guidance document on delivery, treatment planning, and clinical implementation of IMRT: Report of the IMRT subcommittee of AAPM radiation therapy committee," *Medical Physics*, vol. 30, pp. 2089-2115, 2003.
- [4] L. Xing, Q. Wu, Y. Yong, and A. L. Boyer, in *Physics of IMRT and Inverse Treatment Planning in Intensity Modulated Radiation Therapy: A Clinical Perspective*, edited by A. F. Mundt and J. C. Roeske, pp. 20-51, 2005.
- [5] M. J. Murphy, "Tracking Moving Organs in Real Time," *Seminars in Radiation Oncology*, vol. 14, no. 1, pp. 91-100, 2004.
- [6] M. van Herk, "Errors and margins in radiation oncology," *Semin. Radiat. Oncol.* vol. 14, pp. 52-64, 2004.
- [7] J. Hanley *et al.*, "Deep inspiration breath-hold technique for lung tumors: The potential value of target immobilization and reduced lung density in dose escalation," *Int. J. Radiat. Oncol., Biol., Phys.* vol. 45, pp. 603-611, 1999.
- [8] H. D. Kubo *et al.*, "Breathing-synchronized radiotherapy program at the University of California Davis Cancer Center," *Med. Phys.*, vol. 27, pp. 346, 2000.
- [9] S. S. Vedam *et al.*, "Determining parameters for respiration-gated radiotherapy," *Med. Phys.*, vol. 28, pp. 2139-2146, 2001.
- [10] X. A. Li, C. Stepaniak, and E. Gore, "Technical and dosimetric aspects of respiratory gating using a pressure-sensor motion monitoring system," *Med. Phys.*, vol. 33, pp. 145-154, 2006.
- [11] N. Wink *et al.*, "Individualized gating windows based on fourdimensional CT information for respiration gated radiotherapy," *Med. Phys.*, vol. 34, pp. 2384, 2007.
- [12] A. Schweikard *et al.*, "Robotic motion compensation for respiratory movement during radiosurgery," *Comput. Aided Surg.*, vol. 5, pp. 263-277, 2000.
- [13] P. J. Keall *et al.*, "A four-dimensional controller for DMLC-based tumor tracking," *Int. J. Radiat. Oncol., Biol., Phys.*, vol. 60, pp. S338-S339, 2004.
- [14] C. Ozhasoglu, "Synchrony-Real-time respiratory compensation system for the CyberKnife," *Med. Phys.*, vol. 33, pp. 2245-2246, 2006.
- [15] P. J. Keall *et al.*, "Motion adaptive x-ray therapy: A feasibility study," *Phys. Med. Biol.*, vol. 46, pp. 1-10, 2001.
- [16] T. Neicu *et al.*, "Synchronized moving aperture radiation therapy SMART: Average tumor trajectory for lung patients," *Phys. Med. Biol.*, vol. 48, pp. 587-598, 2003.

- [17] L. Papiez, "The leaf sweep algorithm for an immobile and moving target as an optimal control problem in radiotherapy delivery," *Math. Comput. Modell.*, vol. 37, pp. 735-745, 2003.
- [18] H. Shirato *et al.*, "Real-time tumor-tracking radiotherapy," *Lancet*, vol. 353, pp. 1331-1332, 1999.
- [19] Y. Takai *et al.*, "Development of a new linear accelerator mounted with dual fluoroscopy using amorphous silicon flat panel X-ray sensors to detect a gold seed in a tumor at real treatment position," *Int. J. Radiat. Oncol. Biol. Phys.*, vol. 51 (Supple.), pp. 381, 2001.
- [20] R. I. Berbeco *et al.*, "Integrated radiotherapy imaging system IRIS: Design considerations of tumour tracking with linac gantry-mounted diagnostic x-ray systems with flat-panel detectors," *Phys. Med. Biol.*, vol. 49, pp. 243-255, 2004.
- [21] K. R. Britton *et al.*, "Evaluation of inter-and intrafraction organ motion during intensity modulated radiation therapy (IMRT) for localized prostate cancer measured by a newly developed on-board image-guided system," *Radiat. Med.*, vol. 23, pp. 14-24, 2005.
- [22] R. D. Wiersma *et al.*, "Combined kV and MV imaging for real-time tracking of implanted fiducial markers," *Med. Phys.*, vol. 35, pp. 1191-1198, 2008.
- [23] H. D. Kubo and B. C. Hill, "Respiration gated radiotherapy treatment: A technical study," *Phys. Med. Biol.*, vol. 41, pp. 83-91, 1996.
- [24] C. Ozhasoglu and M. J. Murphy, "Issues in respiratory motion compensation during external-beam radiotherapy," *Int. J. Radiat. Oncol., Biol., Phys.*, vol. 52, pp. 1389-1399, 2002.
- [25] L. Simon *et al.*, "Lung volume assessment for a cross-comparison of two breathing-adapted techniques in radiotherapy," *Int. J. Radiat. Oncol., Biol., Phys.*, vol. 63, pp. 602-609, 2005.
- [26] P. R. Winters, "Forecasting Sales by Exponentially Weighted Moving Averages," *Management Science*, vol. 6 pp. 324-342, 1960.
- [27] G. E. P. Box, G. M. Jenkins, *Time Series Analysis, Forecasting and Control*, Holden-Day, pp. 1-553, 1970.
- [28] Hokkaido University Hospital, Sapporo, Japan. <http://www.huhp.hokudai.ac.jp/>
- [29] R. E. Kalman, "A New Approach to Linear Filtering and Prediction Problems," *T. ASME, J. Basic Engineering*, Series D, vol. 83, pp. 35-45, 1961.
- [30] K. Akaike and G. Kitagawa, *Practice in Time Series Analysis I*, Asakura-Shoten, 2003 (in Japanese).
- [31] Peter J. Brockwell and Richard A. Davis, *Introduction to Time Series and Forecasting*, Springer Texts in Statistics, Springer, 1996.
- [32] M. Isaksson *et al.*, "On using an adaptive neural network to predict lung tumor motion during respiration for radiotherapy applications," *Med. Phys.*, vol. 32, no. 12, pp. 3801-3809, 2005.
- [33] M. J. Murphy and S. Dieterich, "Comparative performance of linear and nonlinear neural networks to predict irregular breathing," *Phys. Med. Biol.*, vol. 51, pp. 5903-5914, 2006.
- [34] Hazem M. El-Bakry and Nikos Mastorakis, "A New Fast Forecasting Technique using High Speed Neural Networks," *WSEAS Trans. Signal Processing*, vol. 4, issue 10, pp. 573-595, 2008.
- [35] Sanjay L. Badjate and Sanjay V. Dudul, "Multi Step Ahead Prediction of North and South Hemisphere Sun Spots Chaotic Time Series using Focused Time Lagged Recurrent Neural Network Model," *WSEAS Trans. Information Science and Applications*, vol. 6, issue 4, pp. 684-693, 2009.
- [36] Miguel A. Garcia and Francisco Rodriguez, "An Iterative Algorithm for Automatic Fitting of Continuous Piecewise Linear Models," *WSEAS Trans. Signal Processing*, vol. 4, issue 8, pp. 474-483, 2008.